

Agglomeration and chain formation in ferrofluids: Two-dimensional x-ray scattering

Tobias Kruse, Hans-Georg Krauthäuser,* Anna Spanoudaki,† and Rolf Pelster
II. Physikalisches Institut der Universität zu Köln, Zùlpicher Straße 77, 50937 Köln, Germany
 (Received 29 July 2002; published 21 March 2003)

We present a comprehensive study of field-induced anisotropy in ferrofluids using two-dimensional small-angle x-ray scattering. On application of a homogeneous magnetic field, magnetite particles form anisotropic clusters with preferred orientation parallel to the field. The orientation of single nonspherical particles contributes little to structural anisotropy, since their effective axis ratio is only about 1.05. We determine the average radius of particles in clusters to be of the order of the mean particle radius in the ferrofluid, i.e., 4–5 nm. Therefore, particles of all sizes contribute to cluster formation. Since the thermal energy exceeds the magnetic dipole-dipole interaction of small particles, thermally stable clusters cannot form without an additional interaction energy. We show that van der Waals interaction yields a significant contribution that cannot be neglected in polydisperse systems.

DOI: 10.1103/PhysRevB.67.094206

PACS number(s): 61.10.Eq, 61.46.+w, 75.50.Mm, 77.84.Lf

I. INTRODUCTION

The material parameters of heterogeneous materials depend on the properties of their components as well as on their microstructure. This holds for quantities such as elasticity, thermal and electrical conductivity, permittivity, permeability, etc. For the correct interpretation of macroscopic measurements or for tailoring composite materials it is therefore indispensable to know the correlation between structure and effective properties. Exact solutions of the so-called effective-medium problem have been achieved only for simple systems like perfectly ordered arrangements of equally sized spheres. (For the permittivity see Refs. 1 and 2.) However, real systems show more complicated random or nonrandom spatial arrangements that depend on the degree of particle agglomeration. For example, it has been shown that the permittivity of nanoparticles dispersed in a matrix depends systematically on the shape and size distribution of the particles as well as on their spatial distribution.^{3–5} In order to understand the above correlation it is of great interest to study heterogeneous materials, the microstructure of which can be altered via an external parameter while components and mixture ratio remain unchanged. This has motivated our structural and dielectric study of ferrofluids, the results of which are reported here.

Ferrofluids are colloidal dispersions of magnetic monodomain nanoparticles in a carrier liquid.^{6,7} In a magnetic field, the magnetic moments of the particles tend to orient themselves parallel to the field direction following one of two mechanisms: either the particle rotates together with its magnetic moment (Brown orientation⁸) or the particle keeps its orientation but the magnetic moment vector rotates with respect to the crystal structure (Néel orientation⁹). Phase separation and permanent agglomeration are prevented through an organic surfactant layer covering the particles. Nevertheless, attractive dipole-dipole and van der Waals interactions may lead to the formation of clusters. Theoretical investigations, treating ferrofluids as dipolar hard sphere liquids,^{10–14} predict that a strong dipole-dipole interaction leads to the formation of chainlike or ringlike structures, in which the particle magnetic moments are aligned in a nose-

to-tail manner. When an external magnetic field is applied, ferrofluids develop anisotropic properties, e.g., dielectric^{15,16} or optical^{17,18} anisotropy. It is evident that this must be due to a field-induced anisotropic microstructure, i.e., due to the presence of nonspherical units (particles or clusters) having an orientation parallel to the applied magnetic field. Their shape anisotropy has been investigated in ionic ferrofluids using optical- and x-ray-scattering techniques.¹⁹ Anisometric aggregates have been also detected in ferronematics, i.e., in liquid crystals doped with ferrofluids, which were exposed to uniform magnetic fields^{20,21} or magnetic field gradients²² (so-called primary and secondary aggregation or chaining processes). However, the microscopic process of cluster formation is not yet clear. Various microscopic changes might cause anisotropy: (i) formerly well-separated particles form chains or elongated clusters parallel to the applied field, (ii) spherical clusters become nonspherical and elongated (the particle positions change or new particles join the cluster), (iii) nonspherical particles undergo Brownian orientation, or (iv) entire nonspherical clusters orient themselves along the applied field. Another open question is to what extent particles of different sizes contribute to cluster formation: Monte Carlo simulations of monodisperse systems indicate that agglomeration behavior strongly depends on the strength of dipole-dipole interaction²³ and thus on particle size. Accordingly, in real polydisperse ferrofluids mainly larger particles are expected to form clusters.^{24,21}

In this work we study the field-induced formation of anisotropic microstructure in ferrofluids by means of two-dimensional small-angle x-ray scattering (SAXS).²⁵ We focus on the question of how the anisotropy of single particles and clusters contributes to structural anisotropy. Especially, we investigate the size of particles taking part in cluster formation. In a second contribution to follow, we shall use Monte Carlo simulations to evaluate the size and form of clusters. In a third article we shall present dielectric measurements on the same samples²⁶ in order to correlate microstructure and dielectric anisotropy.

II. SAMPLE CHARACTERIZATION

The liquids studied were purchased from Ferrofluidics GmbH (Nürtingen, Germany). They contain magnetite

TABLE I. Saturation magnetization M_S , density ρ_m , and volume fraction f of magnetite as determined by density measurements. For comparison also the producer's data for the volume fraction f_F are shown. However, these values are too low (see text).

Ferrofluid Samples (Ferrofluidics GmbH)				
Sample	M_S (mT)	f (%)	$f_F = \frac{M_S}{M_{bulk}}$ (%)	ρ_m (g/cm ³)
Isopar-m	0	0.0	0.0	0.78
EMG 911	10	2.4	1.7	0.88
EMG 909	20	4.8	3.6	0.98
EMG 905	40	9.9	7.1	1.19
EMG 901a	60	15.0	10.7	1.42

(Fe₃O₄) particles of almost spherical shape²⁷ with a mean diameter of about 10 nm. (For details see below and Sec. III.) The surfactant layer is formed by spacer molecules of oleic acid with a chain length of about 2 nm; the carrier liquid is Isopar-m, an oil. The samples were of the nominal types EMG 901, 905, 909, and 911. Some of their physical properties are presented in Table I. The volume fraction f of magnetite particles has been calculated directly from density measurements. It varies between 0 and 15%. The saturation magnetization M_S ($M = B - \mu_0 H$) increases linearly with increasing f (see Table I): $M_S = f M_p$, with M_p being the mean magnetization of a magnetite particle. With our data we obtain $M_p = 0.4025$ T. This value is considerably lower than that for bulk magnetite,⁶ $M_{bulk} = 0.56$ T. It has been already pointed out that a reduction of magnetization in nanoparticles may be due to either a nonmagnetizable surface layer²⁸ or to lattice tensions.²⁹ For easy reference we have also listed the volume fraction specified by Ferrofluidics, f_F , although these values are too low: they are calculated as $f_F = M_S / M_{bulk}$ neglecting the difference between bulk and nanoparticles. We have determined the size distribution of the particles via x-ray scattering, performed with a Kratky-Camera at a wavelength of 0.145 nm (Cu $K\alpha$ line). Capillary tubes with a diameter of 1 mm and a wall thickness of 0.01 mm were used as sample holders. The samples were diluted to a magnetite volume concentration of ca. 0.2%. This results in an increase of particle distances, so that interference effects are minimized. To process the data we have employed the structure interference method.^{30,31} For all ferrofluids we obtain a rather broad size distribution with a maximum at a radius of about 4.5–5 nm and a half width of about 4–5 nm (see Fig. 1). We do not interpret the small secondary peak at 13–14 nm, since it is not clear whether it is an inherent feature of the size distribution or an artifact due to residual interparticle interference.

III. TWO-DIMENSIONAL SAXS: PARTICLE SHAPE AND CLUSTER FORMATION

The SAXS experiments took place at the JUSIFA beamline at Hazylab, DEZY, Hamburg.³² The bright synchrotron radiation facilitates the use of a point collimation system and thus allowed us to perform two-dimensional measurements

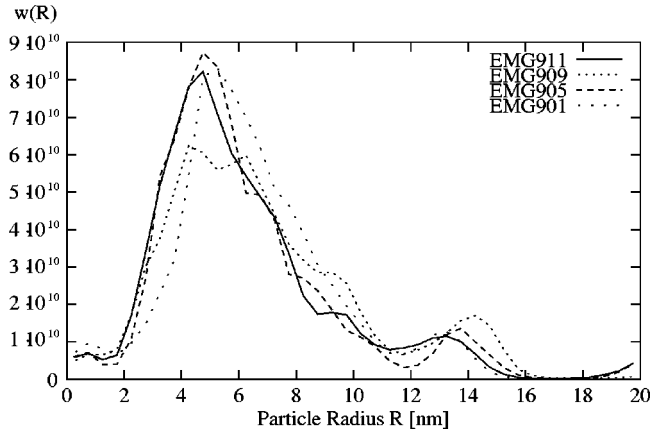


FIG. 1. The size distribution of the magnetite particles. It has been normalized, so that $w(R)dR$ equals the volume fraction of particles with radius R .

(see Fig. 2). The energy of the beam was chosen to be $E = 7.09$ keV (0.174 nm) with a half width of $\delta E/E \approx 10^{-4}$. This is just below the K absorption line of Fe, so that even at particle concentrations up to 15%, the scattered intensity was high enough to be detected. The detector had linear dimensions of 0.2 m and a resolution of 217×217 pixel. In order to cover a range of scattering vectors from $h = 10^{-3}$ to 3×10^{-2} nm each measurement was performed twice with different sample-to-detector distances. The samples were placed in capillary tubes as described above. Using a specially designed sample holder, measurements were conducted in magnetic inductions B from 0 to 0.3 T. The magnetic field direction \hat{x} was perpendicular to the beam direction $-\hat{z}$, as shown schematically in Fig. 2. All measurements were conducted at room temperature. For more details we refer to Ref. 25.

Such two-dimensional measurements yield information on the microstructure of ferrofluids: The scattered intensity $I(\mathbf{h})$ at a scattering vector $\mathbf{h} = (h_x, h_y)$ depends on the distribution of electron density $\rho_e(\mathbf{r})$ in the sample. Except for the

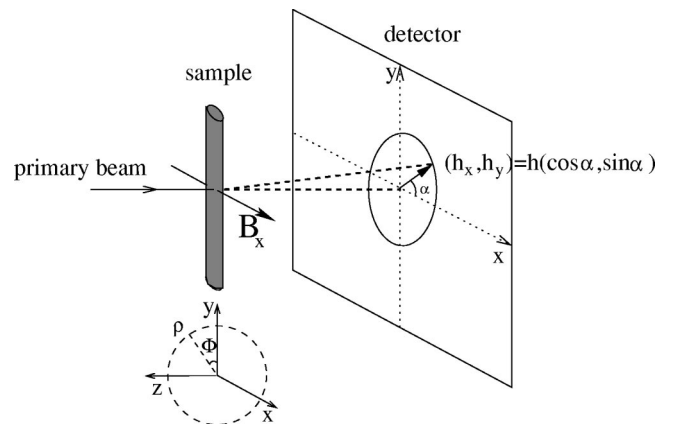


FIG. 2. The geometry of the two-dimensional SAXS measurements, where the samples are exposed to a homogeneous magnetic field. The scattered intensity $I_B(\mathbf{h})$ is function of scattering vector $\mathbf{h} = (h_x, h_y) = h(\cos \alpha, \sin \alpha)$ and magnetic induction B_x . For the spatial coordinates we use both a Cartesian and a cylindrical system [$(x, y, z) \rightarrow (x, \rho, \Phi)$; see text].

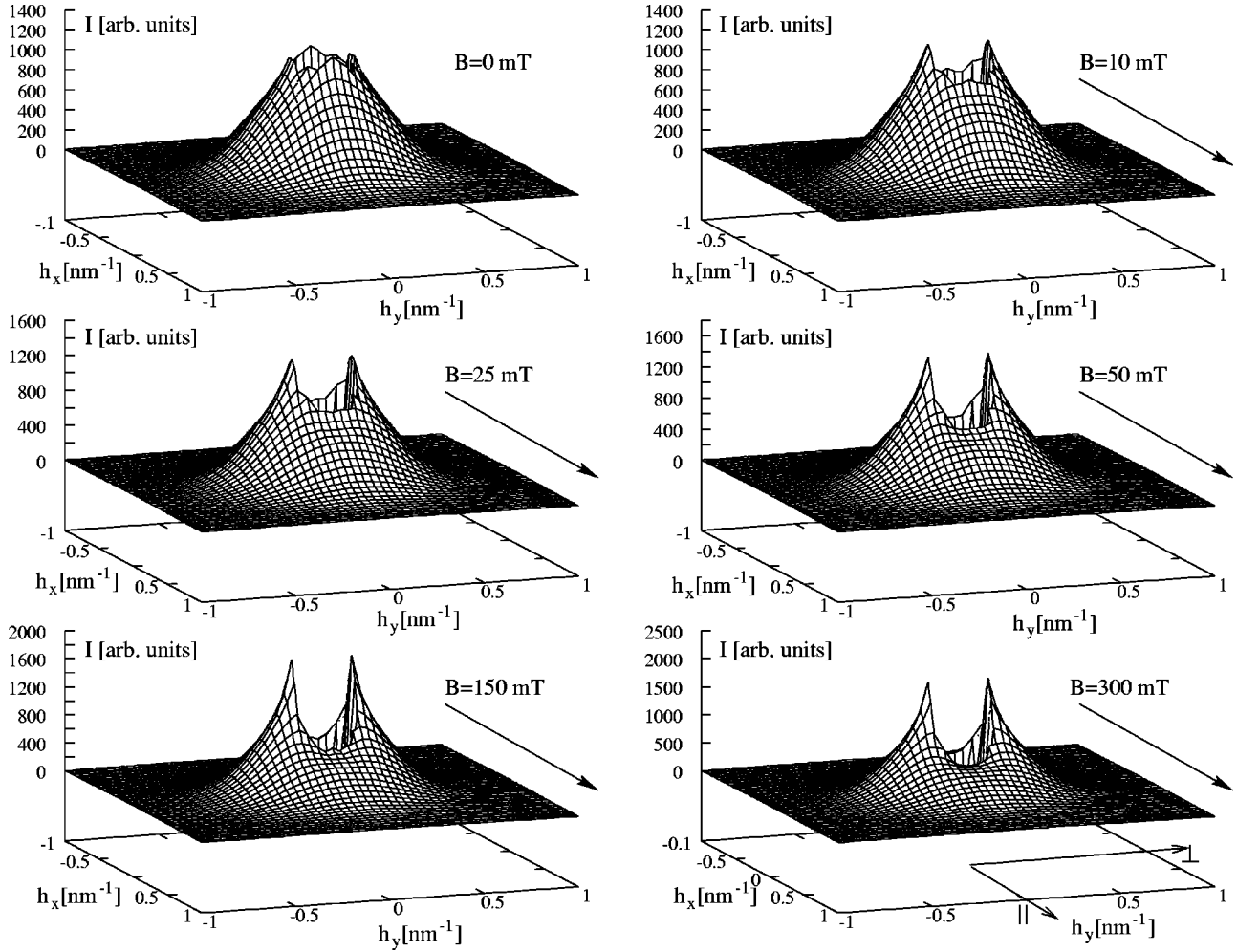


FIG. 3. Two-dimensional plot of the scattered intensity for the sample EMG 905 at different magnetic fields. The range of small scattering vectors, where the intensity of the primary beam dominates, has been cut ($|h| < 0.15 \text{ nm}^{-1}$).

case of forward scattering, $h_x = h_y = 0$, the intensity distribution can be written as

$$I_{h \neq 0}(\mathbf{h}) = I_e \int \gamma(\mathbf{r}) \cos(h_x x) \cos(h_y y) dV, \quad (1)$$

where I_e denotes the scattering intensity of a single electron. The so-called characteristic function or autocorrelation function $\gamma(\mathbf{r}) = \gamma(-\mathbf{r}) = \Delta \varrho_e(\mathbf{r}) * \Delta \varrho_e(-\mathbf{r})$ is the convolution of the electron density contrast, i.e., of the difference between local electron density at a point \mathbf{r} and its volume average: $\Delta \varrho_e = \varrho_e(\mathbf{r}) - \overline{\varrho_e}$. Since the variation of $\varrho_e(\mathbf{r})$ in space is mainly due to the strong contrast between the electron densities of magnetite and carrier liquid, γ and thus the measured intensity reflect the microstructure of the sample.

Figure 3 shows the two-dimensional scattered intensities at different magnetic fields for the sample EMG 905, representatively for all the samples. The intensity at scattering vectors $|h| < 0.15 \text{ nm}^{-1}$ is not shown, since this region is dominated by the primary beam. For $B = 0$ the intensity pattern is isotropic: It does not depend on the direction of $\mathbf{h} = (h_x, h_y) = (h \cos \alpha, h \sin \alpha)$, i.e., on the angle α (see Fig. 2: $\tan \alpha = h_y / h_x$). With increasing magnetic field an anisotropy

develops: The intensity parallel to the field, $I_{\parallel} = I(h, \alpha = 0) = I(h, \alpha = \pi)$ decreases, while it increases in the perpendicular direction, $I_{\perp} = I(h, \alpha = \pm \pi/2)$, so that $I_{\parallel}(h) < I_{\perp}(h)$ holds. This has also been observed in other studies.^{19,33} Our measurements show that the process is fully reversible.

The observed behavior can be understood as follows: On application of a homogeneous magnetic field $B = B_x$, the characteristic function is no longer isotropic, but develops a cylindrical symmetry along the field axis \hat{x} . That is, changing from Cartesian to cylindrical coordinates $(\hat{x}, \hat{\rho}, \hat{\phi})$ where $\rho = \sqrt{y^2 + z^2}$ and $\tan \phi = z/y$; see Fig. 2) Eq. (1) reads

$$\begin{aligned} I_{B; h \neq 0}(\mathbf{h}) &= I_e \int \gamma_B(x, \rho) \cos(h_x x) \\ &\quad \times \left(\int_0^{2\pi} \cos(h_y \rho \cos \phi) d\phi \right) dx \rho d\rho \\ &= 2\pi I_e \int \gamma_B(x, \rho) \cos(h_x x) J_0(h_y \rho) dx \rho d\rho, \end{aligned} \quad (2)$$

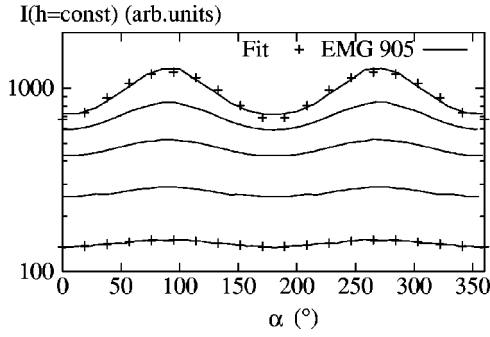


FIG. 4. The angle dependence of the scattered intensity for the sample EMG 905 at $B=0.3$ T. We present the measured data (continuous lines) for scattering vectors (from top to bottom) $h=0.2, 0.3, 0.4, 0.5,$ and 0.6 nm^{-1} , as well as the fitting results according to Eq. (4) for the first and the last case (+).

where J_0 is the Bessel function of the first kind of order zero. Using the above-defined angle α (see Fig. 2), this can be also written in the form

$$I_{B;h \neq 0}(h, \alpha) = 2\pi I_e \int \gamma_B(x, \rho) \cos(h \cos \alpha \cdot x) \times J_0(h \sin \alpha \cdot \rho) dx d\rho. \quad (3)$$

Since both the cosine and the Bessel function are even functions, the intensity pattern exhibits a periodicity $I(h, \alpha) = I(h, \alpha \pm \pi)$. This is shown in Fig. 4, where we display the measured angle dependence $I(h, \alpha)$ at $B=0.3$ T. For a given value of h the scattered intensity oscillates between $I_{\parallel}(h)$ and $I_{\perp}(h)$. Our data can be well fitted by a function of the form

$$I(h, \alpha) = I_0(h) \{1 + A(h)(\sin^2 \alpha - 0.5)\}, \quad (4)$$

where $I_0(h)$ denotes the radial mean value

$$I_0(h) = \frac{I_{\perp}(h) + I_{\parallel}(h)}{2} \quad (5)$$

and

$$A(h) = 2 \frac{I_{\perp}(h) - I_{\parallel}(h)}{I_{\perp}(h) + I_{\parallel}(h)}. \quad (6)$$

A is a measure of anisotropy and depends on B . Summarizing, the two-dimensional (2D) intensity pattern is fully determined by the two profiles parallel and perpendicular to the field axis, $I_{\parallel}(h)$ at $\alpha=0$ and $I_{\perp}(h)$ at $\alpha=\pm\pi/2$. In the following we are going to show that the above 2D measurements in a magnetic field give us information on a possible field-induced orientation of particles as well as on their spatial arrangement.

A. Field-induced orientation of nonspherical particles

Previous transmission electron microscopy (TEM) studies have revealed that the particles are of almost spherical shape.²⁷ On the other hand, measurements of optical birefringence in an ionic ferrofluid revealed a shape anisotropy of about 5% for single particles.¹⁹ Also for the surfacted ferrofluid under study we cannot exclude a restricted asphericity

that would contribute to field-induced structural anisotropy: a portion of these nonspherical particles will tend to orient themselves with their longest axis parallel to the direction of an applied magnetic field (Brownian orientation; see Introduction). Of course, thermal motion as well as the interaction between the magnetic moments of the particles prevents a perfect alignment. In addition, a fraction of small particles does not orient themselves at all since it follows the Néel mechanism of magnetic relaxation. In order to give a microscopic interpretation of field-induced anisotropic properties of ferrofluids, the above partial orientation has to be distinguished from structural changes like cluster or chain formation.

In general, both the scattering of single particles and interparticle interference effects contribute to the measured intensity $I(\mathbf{h})$. The latter are due to multiple scattering between particles and thus reflect the spatial arrangement of the particles. In the limit of large scattering vectors h , though, the intensity pattern is solely determined by single-particle scattering, a process that depends on the shape of the particles. The interparticle interference effects can be neglected. For example, a polydisperse system of spherical particles with radii R_i exhibits an isotropic intensity pattern, even in the presence of field-induced anisotropic clusters. According to Ref. 34,

$$I \propto V_p^2 \langle \Phi^2(hR_i) \rangle_{avg} \quad (7)$$

$$= V_p^2 \frac{9}{(hR_{avg})^4} \quad \text{for } hR_{avg} \gg 1 \quad (8)$$

holds, where V_p is the total volume of all particles, the brackets $\langle \dots \rangle_{avg}$ denote the ensemble average, and the function Φ is the so-called form factor of a sphere. This is an oscillating function in monodisperse systems, but in polydisperse systems the zeros average out and only an envelope remains defining an average radius R_{avg} .

If there were nonspherical particles, the aforementioned partial orientation would result in an anisotropic intensity pattern. In order to describe this effect, we consider a polydisperse system of ellipsoidal particles with semiaxes of length R_i , R_i , and $k_i \cdot R_i$ ($k_i \geq 1$). The intensity scattered by a single ellipsoid depends on its extension in the direction of the scattering vector but the form factor keeps its functional form.³⁴ In other words, Eq. (7) remains valid replacing R_i by $E_i = R_i \sqrt{\sin^2 \Theta_i + k_i^2 \cos^2 \Theta_i}$, where Θ_i is the angle between the scattering vector \mathbf{h} and the long axis of the ellipsoid (obviously $R_i \leq E_i \leq k_i R_i$ holds). Now the ensemble average includes not only the size and shape of the particles but also their orientation with respect to $\mathbf{h} = h(\cos \alpha, \sin \alpha)$ (see Fig. 2), so that Eq. (8) becomes

$$I(h, \alpha) \propto V_p^2 \cdot \frac{9}{\{hE_{avg}(\alpha)\}^4} \quad \text{for } hE_{avg}(\alpha) \gg 1. \quad (9)$$

The average particle extension parallel and perpendicular to an applied magnetic field is given by $E_{\parallel} = E_{avg}(\alpha=0)$ and $E_{\perp} = E_{avg}(\alpha=\pi/2)$. These quantities determine the measured anisotropy, i.e., the above-defined profiles I_{\parallel} and I_{\perp} :

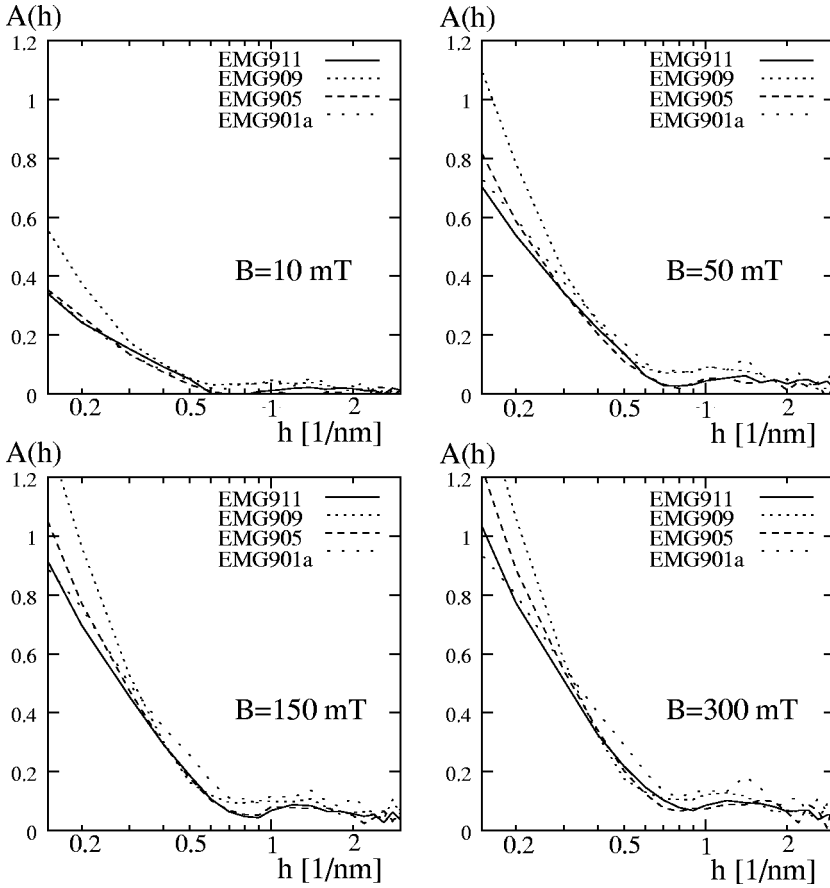


FIG. 5. The anisotropy-related function A according to Eq. (6) vs scattering vector for different magnetic inductions B . For $h > 1 \text{ nm}^{-1}$ only single-particle scattering contributes to the measured intensity and thus A becomes independent of h (see text). The plateau value increases with increasing magnetic induction B until saturation is obtained ($B \geq 0.3 \text{ T}$).

$$I_{\parallel} \propto \frac{1}{(hE_{\parallel})^4} \quad \text{and} \quad I_{\perp} \propto \frac{1}{(hE_{\perp})^4}. \quad (10)$$

Summarizing, the 2D intensity pattern of polydisperse ellipsoids with semiaxis $(R_i, R_i, k_i R_i)$ can be described using the effective semiaxis E_{\parallel} and E_{\perp} : if the particles were completely oriented, $E_{\perp} = R_{avg}$ and $E_{\parallel} = k_{avg} \cdot R_{avg}$ would hold, whereas a random orientation would yield $E_{\parallel} = E_{\perp}$. Thus the effective axis ratio $k_{eff} = E_{\parallel}/E_{\perp}$ is a measure for both the particle orientation and the asphericity: $1 \leq k_{eff} \leq k_{avg}$. The experimental data allow us to determine this ratio. Using Eq. (10) as well as the function A defined in Eq. (6) we obtain

$$k_{eff}(B) = \frac{E_{\parallel}}{E_{\perp}} = \left(\frac{I_{\perp}}{I_{\parallel}} \right)^{1/4} = \left(\frac{1+A/2}{1-A/2} \right)^{1/4} \quad \text{for} \quad hE_{\perp} \geq 1. \quad (11)$$

The effective value of E_{\perp} is of the order of the mean radius of the magnetite particles, i.e., in our case ca. 5 nm (see Fig. 1). Thus Eq. (11) should hold for $h > 5/\bar{R} = 1 \text{ nm}^{-1}$. Indeed, above this limit the anisotropy related function $A(h)$ does not depend anymore on the scattering vector (see Fig. 5). At low B there is no particle orientation, so that $A \approx 0$ for $h > 1 \text{ nm}^{-1}$ and thus $k_{eff}(B=0) = 1$. Increasing the magnetic field the anisotropy becomes visible. At 300 mT saturation is achieved ($B = B_S$) and for large scattering vectors $A \leq 0.1$ holds. According to Eq. (11) we obtain for the effective axis ratio

$$k_{eff} = \frac{E_{\parallel}}{E_{\perp}} \leq 1.05 \quad \text{for} \quad B \geq B_S. \quad (12)$$

As mentioned above, this is a measure for both the particle orientation and the asphericity. For randomly oriented ellipsoids or spheres $k_{eff} = 1$ would hold, whereas $k_{eff} = k_{avg}$ for completely oriented ellipsoids. Thus either the particles have a shape very close to spherical, in accordance with the TEM results, or their mean orientation is weak, so that they contribute little to the measured anisotropy. We shall use this important piece of information later in the interpretation of dielectric measurements.

B. Cluster formation

Before analyzing experimental data, we want to illustrate our previous statement that the characteristic function $\gamma(\mathbf{r})$ contains the complete structural information of a 2D-scattering experiment [Eq. (2)]. As a simple model for an anisotropic cluster system we choose a single dimer consisting of two spheres of radius R at a distance $d_C = 2(R+s)$ from center to center. (In our example $s = 0.2R$.) In the case of ferrofluids, the parameter s corresponds to the thickness of the surfactant layer. The dimer is oriented parallel to the magnetic field axis \hat{x} . We have calculated numerically the convolution $\gamma(\mathbf{r}) = \Delta \varrho_e(\mathbf{r}) * \Delta \varrho_e(-\mathbf{r})$ and display the result in Fig. 6(b) using cylindrical coordinates as defined above [see Eq. (3) and Fig. 2]. γ is the sum of an isotropic and of an anisotropic term. The first one contributes equally in all

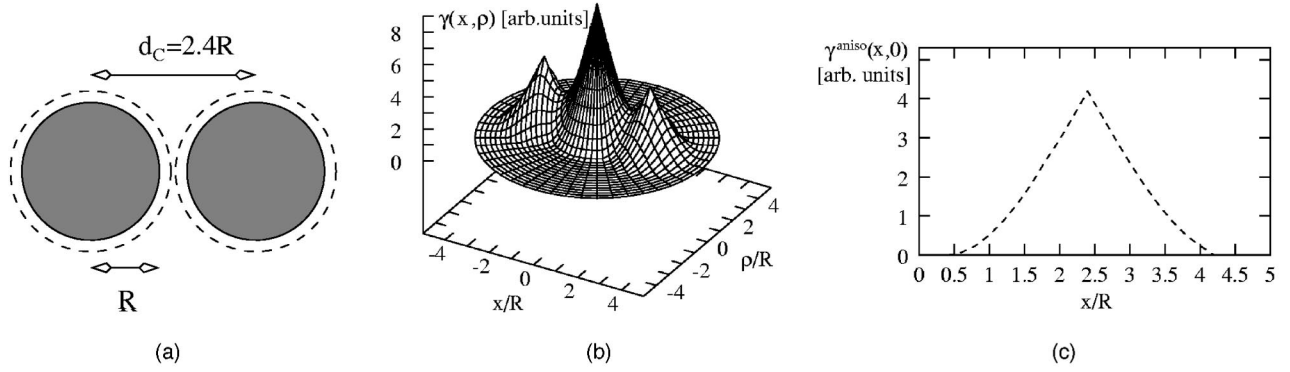


FIG. 6. (a) Two spheres of radius R forming a dimer with orientation parallel to the x axis. The center-to-center distance is $d_C = 2.4R$. (b) Characteristic function of the oriented dimer. For the coordinates x and ρ we refer to Fig. 2 and Eq. (3). (c) Anisotropic contribution of γ in field direction according to Eq. (14). There is maximum autocorrelation at $x = d_C$.

directions while the second one yields no contribution in directions perpendicular to the field axis:

$$\gamma(x, \rho) = \gamma^{iso}(\sqrt{x^2 + \rho^2}) + \gamma^{aniso}(x, \rho),$$

with $\gamma^{aniso}(0, \rho) = 0$. (13)

γ^{iso} gives rise to the symmetric peak in the center and is due to single-particle scattering, while the two smaller peaks (γ^{aniso}) are caused by interparticle interference: They are located at $(x, \rho) = (\pm d_C, 0)$; i.e., they reflect the orientation and extension of the cluster and thus the complete structural information. For a randomly oriented dimer, the interparticle interference would contribute equally in all directions, forming a ring around the central peak. So one way to extract information about structural anisotropy from γ is to evaluate the contribution γ^{aniso} [see Eq. (13)]. This implies identification and subtraction of the 2D function γ^{iso} . But the position of the anisotropy related peaks can also be determined directly in an easy way. According to Eq. (13) the anisotropic contribution in the field direction is

$$\gamma^{aniso}(x, 0) = \gamma(x, 0) - \gamma(0, x); \quad (14)$$

i.e., it can be evaluated calculating the difference of γ along the axes parallel and perpendicular to the field axis. This yields a one-dimensional function with maxima at $x = \pm d_C$ [see Fig. 6(c)].

In the above example, isotropic and anisotropic contributions are well separated and can be easily distinguished [see Fig. 6(b)]. This is much more difficult in real systems such as ferrofluids having complex field-dependent microstructure. Already at $B = 0$, where ferrofluids are isotropic ($\gamma_{B=0}^{aniso} = 0$), there exist clusters of magnetite particles separated by oleic acid spacer molecules. Therefore single-particle scattering and interference between particles in a cluster as well as interference between different clusters will contribute to γ^{iso} . (Note that the latter contribution did not enter the above calculation for a single dimer.) The isotropic contribution results in a broad center peak that can easily mask the smaller side peaks, which form with increasing anisotropy, i.e., with increasing magnetic field. In order to reduce the

isotropic contribution, we show in the following field-induced changes, i.e. [see Eq. (13)],

$$\begin{aligned} \Delta \gamma_B(x, \rho) &= \gamma_B(x, \rho) - \gamma_{B=0}(x, \rho) \\ &= \{\gamma_B^{iso} - \gamma_{B=0}^{iso}\} + \gamma_B^{aniso}(x, \rho) \\ &= \Delta \gamma_B^{iso}(\sqrt{x^2 + \rho^2}) + \gamma_B^{aniso}(x, \rho), \end{aligned}$$

with $\gamma_B^{aniso}(0, \rho) = 0$. (15)

Note that γ and $\Delta \gamma$ only differ in their isotropic term [compare Eqs. (13) and (15)]. The above quantity is evaluated by inverting the difference of the measured scattered intensities with and without applied field, for which according to Eq. (2)

$$\begin{aligned} I_B(\mathbf{h}) - I_{B=0}(\mathbf{h}) &= 2\pi I_e \int \Delta \gamma_B(x, \rho) \cos(h_x x) \\ &\quad \times J_0(h_y \rho) dx d\rho \end{aligned} \quad (16)$$

holds. For the inversion, we use a two-dimensional equidistant discretization of the $(\hat{x}, \hat{\rho})$ space. Figure 7 displays the result of such an inversion for sample EMG 901 at $B = 0.3$ T. There is no central peak at $x = \rho = 0$; i.e., obviously γ^{aniso} dominates and $\Delta \gamma_B^{iso}$ gives only a small contribution [see Eq. (15)]. The two peaks located on the field axis \hat{x}

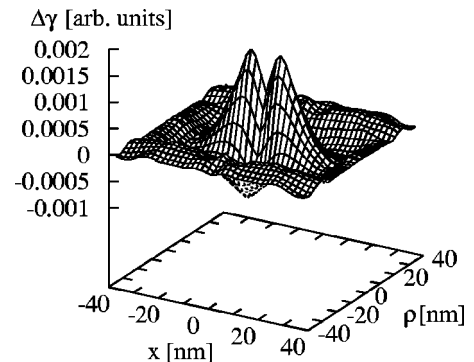


FIG. 7. Two-dimensional plot of the characteristic function after subtraction of symmetric zero-field contributions, $\Delta \gamma_B = \gamma_B - \gamma_{B=0}$ [see Eq. (15)], for sample EMG 901 at $B = 0.3$ T.

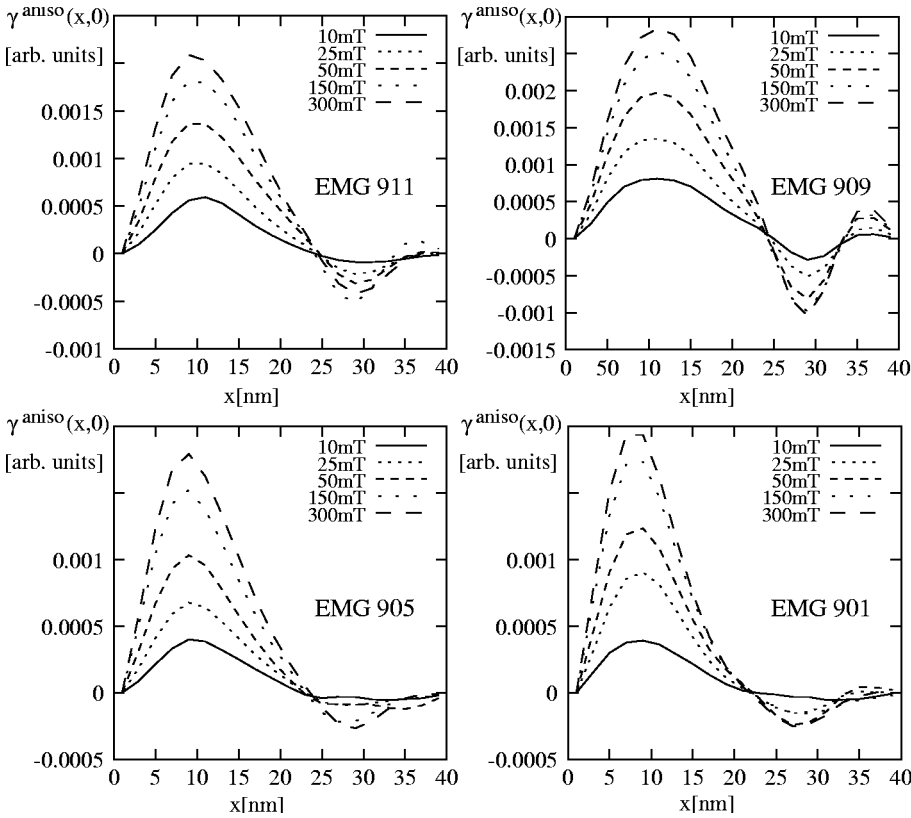


FIG. 8. The anisotropic contribution to the characteristic function along the field axis, $\gamma_B^{aniso}(x,0)$ vs x , according to Eq. (17).

clearly indicate field-induced anisotropy. In order to obtain information on field-induced anisotropy, we have to get rid of remaining symmetric contributions ($\Delta\gamma_B^{iso} \neq 0$). We therefore calculate the anisotropic contribution along the field axis. According to Eq. (15)

$$\gamma_B^{aniso}(x,0) = \Delta\gamma_B(x,0) - \Delta\gamma_B(0,x) = \gamma_B(x,0) - \gamma_B(0,x) \quad (17)$$

holds [for the second equality see Eq. (14)]. So either the difference of $\Delta\gamma_B$ along the x and ρ axis or that of γ_B can be used for the evaluation. [This is due to the fact that γ and $\Delta\gamma$ exhibit the same anisotropic term; see Eqs. (14) and (15).] The result is displayed in Fig. 8. We find for all samples (filling factors) and field strengths a characteristic peak at $x \approx 10$ nm. In contrast to the simple model we have discussed at the beginning of this section, this peak does not necessarily indicate the existence of oriented dimers, but more generally of nonspherical clusters having a preferred orientation parallel to the applied field. What we observe is maximum anisotropic autocorrelation at a distance of 10 nm. Ferrofluids exhibit a disordered microstructure where the autocorrelation of next neighbors dominates. Therefore, we can interpret the above value as the mean center-to-center particle distance in oriented clusters:

$$\overline{d_c} \approx 10 \text{ nm}. \quad (18)$$

Here we content ourselves with an approximative picture of chainlike structures (dimers, trimers, etc.). In order to get more detailed information about field-induced cluster formation, such as cluster size (number of particles) and cluster

form (shape anisotropy), we would have to analyze not only the main peak positions, but the complete form of the characteristic function displayed in Figs. 7 and 8. This might be possible in diluted systems, where γ can be interpreted and modeled as an intracluster autocorrelation function. In our systems with filling factors from 2.4% to 15%, however, interference between different clusters cannot be neglected and thus any further analysis would require a rather sophisticated modelization. For this reason we also do without an approximative evaluation of the cluster form via a Guinier analysis of scattering curves (as has been done, for example, for an ionic ferrofluid revealing bundlelike aggregates; see Ref. 19). We shall address this open question in a second study using Monte Carlo simulations.

Instead of this, we shall now use the above result, Eq. (18), to estimate the mean size of the particles that take part in the field-induced formation or orientation of anisometric clusters. In a cluster neighboring particles are separated by their surface layers of oleic acid spacer molecules having a chain length of 2 nm. But the effective length can be well lower than that.³⁵ Furthermore, the inverted micelle structure in which the oleic acid molecules are organized leaves enough free volume for a partial interpenetration of adjacent layers. TEM studies of ferrofluids show that in clusters of magnetite particles, the surface-to-surface distances can be as small as 0.7 nm (Ref. 27) since, at least after removal of the carrier liquid, the surfactant chains can be tilted or entangled. Therefore, the distance $2s$ between the particle surfaces lies in the range 0.7–4 nm. Using Eq. (18) we obtain a mean radius $\overline{R_C}$ of the particles taking part in cluster formation:

$$\bar{R}_C = \frac{\bar{d}_C - 2s}{2} \approx 3.0\text{--}4.7 \text{ nm.} \quad (19)$$

The above values of d_C and R_C are independent of both the filling factor and the strength of the applied magnetic field (see Fig. 8). Summarizing, we have two main results.

(i) The average particle radius in oriented anisometric clusters is of the order of the mean particle radius $\bar{R} \approx 4\text{--}5$ nm of the ferrofluid (see Fig. 1). At first glance this seems surprising, since bigger particles with a higher magnetic dipole-dipole interaction should have an enhanced probability to form aggregates (see below). But obviously particles of all sizes contribute to cluster formation; i.e., the polydisperse system does not split up into smaller single particles and larger agglomerating particles.

(ii) Although structural anisotropy develops with increasing magnetic field (see Figs. 3 and 8), the average particle radius in oriented anisometric clusters remains constant. Either the applied field mainly induces orientation of already existing aggregates or at every stage of cluster formation small and large particles are involved.

C. Interaction energies and microstructure

Interaction energies in ferrofluids depend on both the particle distances and on their radii. In general, the long-range magnetic dipole-dipole interaction is thought to be responsible for the formation of clusters. Let us consider particles with parallel magnetic dipole moments, e.g., at saturation magnetization. For two particles of radius R_1 and R_2 at a center-to-center distance d_C , the interaction energy is

$$E_{\parallel}^{dd} = -2 \frac{\mu_0}{4\pi} \frac{\mu_1 \mu_2}{d_C^3} \propto \left(\frac{R_1 R_2}{d_C} \right)^3, \quad (20)$$

where $\mu_i = \frac{4}{3} \pi (M_p / \mu_0) R_i^3$ denotes the magnetic dipole moment of particle i and M_p its saturation magnetization. For small particles the dipole-dipole interaction is less important and thus larger particles should have a stronger tendency to form clusters.²¹ The agglomeration behavior is often characterized in terms of an aggregation parameter λ , i.e., the ratio of the magnetic dipole-dipole interaction of two particles and their thermal energy:

$$\lambda = \frac{1}{2} \frac{|E_{\parallel}^{dd}|}{k_B T}. \quad (21)$$

For example, Monte Carlo simulations of monodisperse systems show a transition in the agglomeration behavior with increasing λ , i.e., with decreasing temperature or increasing particle size (see, e.g., Ref. 23).

Above we have shown that the average radius of particles in oriented clusters roughly equals the mean particle radius of the ferrofluid (4–5 nm). For a pair of such small particles ($R_1 = R_2 = 4.5$ nm) at a distance $\bar{d}_C = 10$ nm we obtain with $M_p = 0.4025$ T (see Sec. II)

$$|E_{\parallel}^{dd}| \approx 3 \times 10^{-21} \text{ J} \approx 0.019 \text{ eV.} \quad (22)$$

This is less than the thermal energy at room temperature, $k_B T = 0.025$ eV. Obviously, a dipole-dipole interaction would not be sufficient to achieve a thermally stable cluster. In terms of the above aggregation parameter this reads

$$\bar{\lambda} \approx 0.37. \quad (23)$$

Thermal stability requires at least $\lambda \geq 1$. As a consequence, such small particles can only form aggregates with big particles. In order to estimate down to which particle size this is possible, we rewrite Eq. (21) as

$$\lambda = \left(\frac{R_1 R_2}{R_{limit} d_C} \right)^3, \quad (24)$$

where

$$R_{limit} = \left(\frac{\mu_0 9 k_B T}{4 \pi M_p^2} \right)^{1/3}. \quad (25)$$

In our case $R_{limit} = 2.8$ nm holds at room temperature. Small particles with $R_1 \leq R_{limit}$ can never form a cluster with $\lambda \geq 1$, whatever the size of the second particle is [$R_2/d_C < 1$ in Eq. (24)]. The higher we set the criterion for thermal stability, the larger the portion of particles that can never achieve the required dipole-dipole interaction (i.e., all particles with $R_1 \leq \lambda^{1/3} R_{limit}$). Now let us consider a typical particle with radius $R_1 = \bar{R} = 4.5$ nm. In order to achieve $\lambda \geq 1$ it has to come sufficiently close to a second particle with $R_2 > 9$ nm, for $\lambda \geq 4$ even $R_2 > 440$ nm (for our surfacted particles we have set $d_C \geq R_1 + R_2 + 1$ nm). According to the measured size distribution (Fig. 1) such an interaction can only be obtained with a small portion of particles; i.e., most of the particles would not find a partner to form a stable cluster. Therefore, we would expect to find more likely big particles in a cluster. In addition, the λ dependence of agglomeration behavior observed in Monte Carlo simulations of monodisperse systems has led to the idea that a polydisperse system can be divided into two parts, i.e., into small single particles and larger particles forming definitely aggregates.²¹ But our experimental result indicates that particles of all sizes contribute to the formation of clusters. Obviously, the above energy criterion based solely on the dipole-dipole interaction [Eq. (21)] is too simple, at least for such a polydisperse system. Another mechanism has to provide additional bonding energy:

In clusters with short surface-to-surface distances ($2s = d_C - R_1 - R_2$) the van der Waals interaction can be much stronger than the magnetic dipole-dipole interaction and

$$E_{vdW} = -\frac{A_H}{6} \left\{ \frac{2R_1 R_2}{d_C^2 - (R_1 + R_2)^2} + \frac{2R_1 R_2}{d_C^2 - (R_1 - R_2)^2} + \ln \left(\frac{d_C^2 - (R_1 + R_2)^2}{d_C^2 - (R_1 - R_2)^2} \right) \right\} \quad (26)$$

holds,³⁶ whereas the Hamaker constant A_H has a value in the range from 3×10^{-20} J to 3×10^{-19} J, i.e., from 0.19 eV to 1.9 eV.^{37,6} As in the above example, Eq. (22), we consider particles of typical size $R_1 = R_2 = \bar{R} = 4.5$ nm and $d_C = 10$ nm. With $A_H \geq 0.19$ eV we obtain

$$|E_{vdW}| \geq 4.5 \times 10^{-21} \text{ J} \approx 0.028 \text{ eV} \quad (27)$$

so that $|E_{vdW}| > |E_{\parallel}^{dd}|$ holds [see Eq. (22)]. Agglomeration behavior depends on the total interaction energy, i.e., here $|E_{vdW} + E_{\parallel}^{dd}| \geq 0.047 \text{ eV}$. Now the generalized aggregation parameter indicates thermal stability even at room temperature:

$$\lambda_{total} = \frac{|E_{vdW} + E_{\parallel}^{dd}|}{2k_B T} \approx 1. \quad (28)$$

λ_{total} still depends on particle size ($\lambda_{total} \gg 1$ for big particles), but now also clusters consisting of smaller particles can achieve a sufficient thermal stability.

Summarizing, thermal energy and dipole-dipole interactions govern the microstructure of ferrofluids at long particle distances, i.e., at the first stage of cluster formation. Once small particles come closer, they can only form a thermally stable cluster if there is an additional interaction energy. We have shown that the van der Waals interaction can yield a significant contribution. Of course, the stability of aggregates may also depend on microscopic processes such as the entanglement of spacer molecules, so that particle coating and carrier liquid can be important parameters. Our experiments do not allow us to develop a comprehensive microscopic model for the agglomeration process. Therefore, we content ourselves with the statement that at least the van der Waals interaction should not be neglected in theoretical models or computer simulations describing polydisperse systems.

IV. CONCLUSIONS

We have used two-dimensional SAXS to study the microstructure of ferrofluids. On application of an external homo-

geneous magnetic field, the scattering pattern becomes anisotropic. The orientation of nonspherical particles yields only a small contribution. We have determined an effective axis ratio $k_{eff} = 1.05$ at $B = B_S$; i.e., either the mean orientation is weak or the particle shape is close to the spherical one. Field-induced structural anisotropy is mainly due to the formation and/or orientation of elongated clusters with preferred alignment parallel to the field. We have determined the mean interparticle distance in these clusters, which was found to be ca. 10 nm, independent of filling factor and magnetic field. Thus, the average radius of particles taking part in cluster formation is of the order of the mean radius of all particles (4–5 nm). This indicates that particles of all sizes contribute to cluster formation, although the thermal energy exceeds the magnetic dipole-dipole interaction of small particles. We conclude that although the long-range dipole-dipole interaction is responsible for the particles approaching each other in the initial stage of cluster formation, an additional interaction is necessary to achieve thermally stable clusters. We have shown that the van der Waals interaction gives a significant contribution that should not be neglected in theoretical models or computer simulations describing the agglomeration behavior of polydisperse systems.

ACKNOWLEDGMENTS

The authors are grateful to Professor Dr. Günter Nimtz for hosting this work in his laboratory and for numerous stimulating discussions. The project was supported by the European Commission under TMR Marie Curie Grant No. ERBFMBICT982913 (A.S.) and by the DFG under Project No. Ni/49/33-1.

*Present address: Institut für Grundlagen der Elektrotechnik und elektromagnetische Verträglichkeit, Otto-von-Guericke-Universität Magdeburg, Postfach 4120, 39016 Magdeburg, Germany.

†Present address: Laboratoire de Physique, Ecole Normale Supérieure de Lyon, 46, Allée d'Italie, Lyon Cedex 07, France.

¹K. Günther and D. Heinrich, *Z. Phys.* **185**, 345 (1965).

²D. R. McKenzie, R. C. McPhedran, and G. H. Derrick, *Proc. R. Soc. London, Ser. A* **362**, 211 (1978).

³R. Pelster and U. Simon, *Colloid Polym. Sci.* **277**, 2 (1999).

⁴R. Pelster, *Phys. Rev. B* **59**, 9214 (1999).

⁵A. Spanoudaki and R. Pelster, *Phys. Rev. B* **64**, 064205 (2001).

⁶R. E. Rosensweig, *Ferrohydrodynamics* (Cambridge University Press, New York, 1985).

⁷S. Odenbach, *Adv. Colloid Interface Sci.* **46**, 263 (1993).

⁸W. Fuller Brown, Jr., *Phys. Rev.* **130**, 1677 (1963).

⁹L. Néel, *Ann. Geophys. (C.N.R.S.)* **5**, 99 (1949).

¹⁰I. Jacobs and C. Bean, *Phys. Rev.* **100**, 1060 (1955).

¹¹P. G. de Gennes and P. A. Pincus, *Phys. Kondens. Mater.* **11**, 189 (1970).

¹²P. C. Jordan, *Mol. Phys.* **25**, 961 (1973).

¹³A. S. Clarke and G. N. Patey, *J. Chem. Phys.* **100**, 2213 (1995).

¹⁴P. J. Camp and G. N. Patey, *Phys. Rev. E* **62**, 5403 (2000).

¹⁵B. Z. Kaplan and D. M. Jacobson, *Nature (London)* **259**, 654 (1976).

¹⁶A. J. Mailfert and B. Nahounou, *IEEE Trans. Magn.* **MAG-16**, 254 (1980).

¹⁷H. W. Davies and J. P. Llewellyn, *J. Phys. D* **13**, 2327 (1980).

¹⁸N. A. Yusuf, A. Ramadan, and H. Abu-Safia, *J. Magn. Magn. Mater.* **184**, 375 (1998).

¹⁹M. F. da Silva and A. M. Figueiredo Neto, *Phys. Rev. E* **48**, 4483 (1993).

²⁰C. Y. Matuo, F. A. Tourinho, and A. M. Figueiredo Neto, *J. Magn. Magn. Mater.* **122**, 53 (1993).

²¹K. I. Morozov, *Phys. Rev. E* **66**, 011704 (2002).

²²C. Y. Matuo and A. M. Figueiredo Neto, *Eur. Phys. J. E* **60**, 1815 (1999).

²³A. F. Pshenichnikov and V. V. Mekhonoshin, *Eur. Phys. J. E* **6**, 399 (2001).

²⁴S. Odenbach and H. Störk, *J. Magn. Magn. Mater.* **183**, 188 (1998).

²⁵T. Kruse, Ph.D. thesis, Universität zu Köln, Köln, 2000.

²⁶A. Spanoudaki, Ph.D. thesis, Universität zu Köln, Köln, 2002.

²⁷J. Popplewell and L. Sakhnini, *J. Magn. Magn. Mater.* **149**, 72 (1995).

²⁸R. Kaizer and G. Miscolczy, *J. Appl. Phys.* **42**, 1064 (1970).

²⁹C. Johansson, M. Hansson, M. S. Pedersen, and S. Morup, *J. Magn. Magn. Mater.* **173**, 5 (1997).

³⁰H. G. Krauthäuser and G. Nimtz, *J. Mol. Struct.* **383**, 315 (1996).

- ³¹H.-G. Krauthäuser, Ph.D. thesis, Universität zu Köln, Köln, 1996.
- ³²H.-G. Haubold *et al.*, Rev. Sci. Instrum. **60**, 1943 (1989).
- ³³J. Lal, D. Abernathy, L. Auvray, O. Diat, and G. Grübel, Eur. Phys. J. E **4**, 263 (2001).
- ³⁴J. S. Pedersen, Adv. Colloid Interface Sci. **70**, 171 (1997).
- ³⁵J. N. Israelachvili, *Intermolecular and Surface Forces* (Academic Press, San Diego, 1985).
- ³⁶*Dispersion Forces*, edited by J. Mahanty and B. W. Ninham (Academic Press, New York, 1976).
- ³⁷L. N. Donselaar, P. M. Frederik, P. Bomans, P. A. Buining, B. M. Humbel, and A. P. Philipse, J. Magn. Magn. Mater. **201**, 58 (1999).